materials

MDPI

Article

High Efficient Reduction of Graphene Oxide via Nascent Hydrogen at Room Temperature

Qiqi Zhuo [1], Jijun Tang [1], Jun Sun [2] and Chao Yan [1,*]

[1] College of Material Science & Engineering, Jiangsu University of Science and Technology, 2 Meng-Xi Road, Zhenjiang 212003, China; zqq88263268@just.edu.cn (Q.Z.); tangjijunnju@126.com (J.T.)

[2] College of Chemistry, Chemical Engineering and Material Science, Soochow University, 199 Ren-Ai Road, Suzhou 215123, China ; sunjun@suda.edu.cn

* Correspondence: chaoyan@just.edu.cn; Tel.: +86-512-8440-8597

Received: 25 January 2018; Accepted: 22 February 2018; Published: 27 February 2018

Abstract: To develop a green and efficient method to synthesize graphene in relative milder conditions is prerequisite for graphene applications. A chemical reducing method has been developed to high efficiently reduce graphene oxide (GO) using Fe_2O_3 and NH_3BH_3 as catalyst and reductants, respectively. During the process, environmental and strong reductive nascent hydrogen were generated surrounding the surface of GO sheets by catalyst hydrolysis reaction of NH_3BH_3 and were used for reduction of GO. The reduction process was studied by ultraviolet absorption spectroscopy, Raman spectroscopy, and Fourier transform infrared spectrum. The structure and morphology of the reduced GO were characterized with scanning electron microscopy and transmission electron microscopy. Compared to metal (Mg/Fe/Zn/Al) particles and acid system which also use nascent hydrogen to reduce GO, this method exhibited higher reduction efficiency (43.6%). Also the reduction was carried out at room temperature condition, which is environmentally friendly. As a supercapacitor electrode, the reversible capacity of reduced graphene oxide was 113.8 F g^{-1} at 1 A g^{-1} and the capacitance retention still remained at 90% after 200 cycles. This approach provides a new method to reduce GO with high reduction efficiency by green reductant.

Keywords: graphene oxide; graphene; reductants

1. Introduction

Graphene has gained large attention because of its excellent mechanical, electrical, thermal and optical properties. Special electronic structure and outstanding properties provide graphene with great potential in the applications of sensors [1–3], electronics [4–6], batteries [7,8], and nanocomposites [9–11]. Thus, a facile synthesis of graphene with large quantities is pursued. To date, many techniques have been introduced to synthesize graphene, such as chemical reduction of GO [12–15], liquid-phase exfoliation [16,17], micro-mechanical exfoliation [18], chemical vapor deposition [19–21], etc. Overall, the chemical reduction of GO is believed to be one of the most promising methods to synthesize reduced graphene oxide (r-GO) with low cost and large-scale productivity [14]. Until now, the graphene oxide can be large scale prepared by exfoliation of graphite oxide, which is obtained by oxidizing graphite using oxidants and strong acid [22,23]. GO nanosheets have a lot of functional groups—including epoxide, carbonyl, hydroxyl, and carboxy groups—which make it hydrophilic [24,25]. Therefore, GO sheets can be dispersed uniformly in water and many kinds of organic solvent due to electrostatic repulsion of carboxylate groups on GO sheets that with a negative charge [14]. However, metal ions can neutralize the charges on the GO sheets and destabilize the resulting dispersions [26]. For instance, NaCl would make hydrophilic GO aggregate in water [27].

Until now, various inorganic and organic reductants have been exploited for chemical reduction of GO [13,14]. For instance, hydrazine and its derivatives [24] are effective and efficient reductants

for GO reduction [14]. However, these reductants are highly toxic to both living organisms and the environment which limited their usage [28]. Meanwhile, some relatively low-toxicity reductants like hydroxylamine [29], $NaBH_4$ [12,30], urea [31], sugar [32], L-ascorbic acid [33], and sodium citrate [34] are developed for reduction of GO. However, most of these reductants should be employed at a relatively high temperature beyond 90 °C, which will increase the defects in r-GO sheets as examined by Raman spectroscopy and X-ray photoelectron spectroscopy [33]. It is worthwhile to exploit a green and efficient method to prepare graphene from reducing of GO in relative milder conditions. Recently, many studies have focused on chemically reducing GO by green reductants at room temperature. As a strong reducing and environmentally benign agent [14], nascent hydrogen can be used for efficiently reducing of GO. Usually, nascent hydrogen was generated by reaction of acid solution with metal powders. Until now, GO has been reported to be reduced by nascent hydrogen generated by metals of different electrochemical potential (−0.44 V for Fe [35], −0.76 V for Zn [36], −1.66 V for Al [37], −2.37 V for Mg [38]) However, hydrophobic metal powders and hydrophilic GO cannot contact well. A great amount of nascent hydrogen generated around metal powders surface would quickly form non-reducing hydrogen instead to reduce GO, which results in low reduction efficiency.

Ammonia borane (NH_3BH_3) is a stable material for chemically storing hydrogen and an excellent reducing agent [14]. Nascent hydrogen can be generated by release of hydrogen atoms from NH_3BH_3 through methanolysis [39,40] or hydrolysis [41,42] in solution. Compared to the thermal dehydrogenation process which requires high temperature, NH_3BH_3 can release hydrogen at room temperature by hydrolysis reaction with the presence of noble or non-noble metal catalysts (Co. [43], Ru [44], Pd [45], etc.). In our previous work, Co_3O_4 was used as catalyst for high efficient reduction of GO by the hydrolysis of NH_3BH_3. The catalytic rate for NH_3BH_3 hydrolysis of Co_3O_4 is as high as 3~5 times of Fe_2O_3 and about 10~20 times of CuO/Cu_2O [46]. However, the high reaction rate would generate large quantity of nascent hydrogen too fast, thus harming the formation of porous graphene and reducing the capacitance of graphene nanomaterial, which limits its application in the fields of supercapacity. Also, the large amount hydrogen produced in a short time may present some security risks.

Based on the salting out effect of GO, this work describe a mild method for the reduction of GO using nascent hydrogen generated by NH_3BH_3 and Fe_2O_3 as the reducing agent and catalyst, respectively. UV-vis absorption spectroscopy, Raman spectroscopy, and Fourier transform infrared spectrum were used to study the reducing process. The structure and morphology of the reduced graphene oxide were characterized by scanning electron microscopy (SEM) and transmission electron microscopy (TEM). This method showed higher nascent hydrogen reduction efficiency and relatively lower defects than metal/acid reduction system. Besides, supercapacitor with the prepared r-GO materials as electrode was fabricated to study their electrochemical properties.

2. Materials and Methods

2.1. Materials

NH_3BH_3, $FeCl_3$ and HCl were purchased from Sinopharm Chemical Reagent, Shanghai, China. GO was prepared by the modified Hummers method [22].

2.2. Reduction of GO

Firstly, as-prepared GO was dispersed in deionized water by ultrasonic treatment for 30 min to form a homogeneous aqueous solution (0.1 mg/mL). 1 mL of 0.1 M $FeCl_3$ and 10 mg NH_3BH_3 were added to the 10 mL GO (1 mg) solution in sequence. After a 60 min reaction, a black suspension solution was obtained. Finally, the product was followed by washing with dilute HCl and deionized water five times.

2.3. Characterization

Raman spectra were carried out using a Renishaw Micro-Raman spectrometer System, UK with an excitation source of 532 nm wavelength incident laser. UV-vis absorption spectroscopy detection was performed by a LAMBDA 750 spectrometer (PerkinElmer, Waltham, MA, USA). The transmission electron microscopy (TEM, FEI, Hillsboro, OR, USA) was used to investigate surface morphology of r-GO/Fe_2O_3 and r-GO with an accelerating voltage of 200 kV. Fourier transform infrared (FTIR) spectra of the samples were carried with HYPERION 2000 spectrometer (Bruker, karlsruhe, Germany) in the range of 600–4000 cm^{-1}.

2.4. Electrochemical Measurements

The electrochemical performances of r-GO and GO were evaluated using a three-electrode setup in 2 M KOH solution. Pt foil, Hg/HgO, and the as-prepared materials were used respectively as counter electrode, reference electrode, and working electrode. The working electrode was prepared by coating a paste onto nickel foam, using r-GO as active material, poly(tetrafluoroethylene) as binder, and acetylene black as conductive additive with a weight ratio of 80: 10: 10 in NMP. Finally, the nickel foam was dried at 80 °C and the weight of active material on each electrode was about 1.5 mg.

3. Results and Discussion

3.1. Schematic of Reduction Process

Figure 1 shows the schematic of the reducing GO. Due to ionization of the carboxylic acid and phenolic hydroxyl groups on the GO sheets, GO sheets shows highly negative charge when dispersed in water. $FeCl_3$ solution would neutralize the negative charge of GO after adding to the GO solution, thus make GO sheets agglomerate. Then NH_3BH_3 was added and a black suspension of r-GO/Fe_2O_3 was obtained. Fe_2O_3 NPs could catalyze the hydrolysis reaction of NH_3BH_3 to generate nascent hydrogen to reduce GO nanosheets. At last, Fe_2O_3 nanoparticles were removed away by HCl and the pure r-GO was collected.

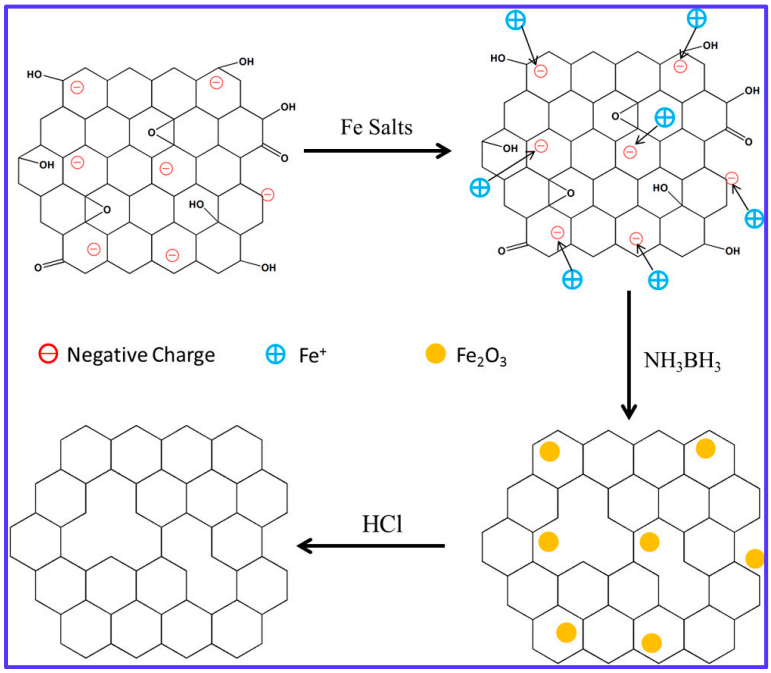

Figure 1. Schematic of reducing GO sheets.

3.2. Structural and Morphological Investigations

Ultraviolet visible spectroscopy was used to study the reduction process. The ultraviolet visible absorption peak of GO/$FeCl_3$ solution shifted from 232 nm (Figure 2a) to 268 nm (Figure 2b) after 30 min, and the solution color changed from brown to black, indicating that the highly conjugated structure like that of graphite was formed gradually and GO was reduced to graphene [12,32,35]. Compared to the system of GO/$FeCl_3$, the reduction rate of pure GO without $FeCl_3$ was much slower. Meanwhile, the solution color did not have obvious change with the reaction time extended even to 60 min (Figure 2d). This result demonstrated that iron salts can work as the catalyst to accelerate the hydrolysis reaction of NH_3BH_3 greatly to generate nascent hydrogen and reduce GO. Below showed the reduction process of GO:

$$NH_3BH_3 + 2H_2O \xrightarrow{Fe_2O_3} NH_4^+ + BO_2^- + 6H \quad (1)$$

$$GO + aH \longrightarrow r - GO + bH_2O + cH_2 \quad (2)$$

In the first step, Fe_2O_3 NPs were absorbed on the surface of GO and then a mass quantity of nascent hydrogen formed around the Fe_2O_3 NPs by the hydrolysis of NH_3BH_3, which could be directly used to reduce GO. In the second step, GO was reduced by nascent hydrogen.

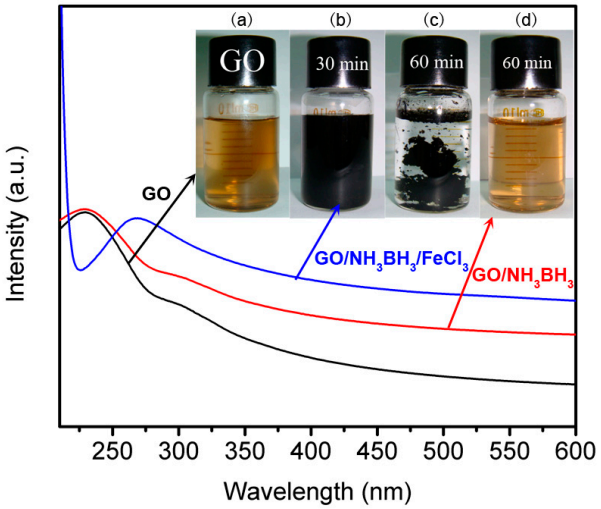

Figure 2. Ultraviolet visible spectroscopy of GO (**a**) and GO/NH_3BH_3 with (**b** for 30 min, **c** for 60 min) or without (**d**) $FeCl_3$ during the reduction process. Inset picture is the corresponding photos of the products.

Figure 3 shows the SEM image of r-GO/Fe_2O_3 NPs with different magnifications. There are numerous Fe_2O_3 NPs decorated on r-GO sheets. Corresponding EDX result indicated the existence of Fe, O, and C elements. The morphology was also characterized by TEM as shown in Figure 4. It is clearly seen that the Fe_2O_3 NPs disperse uniformly on the r-GO sheets (Figure 4b). No nanoparticles can be seen on pure GO sheets (Figure 4a). After being washed with HCl, Fe_2O_3 NPs were removed completely and pure r-GO was obtained (Figure 4c).

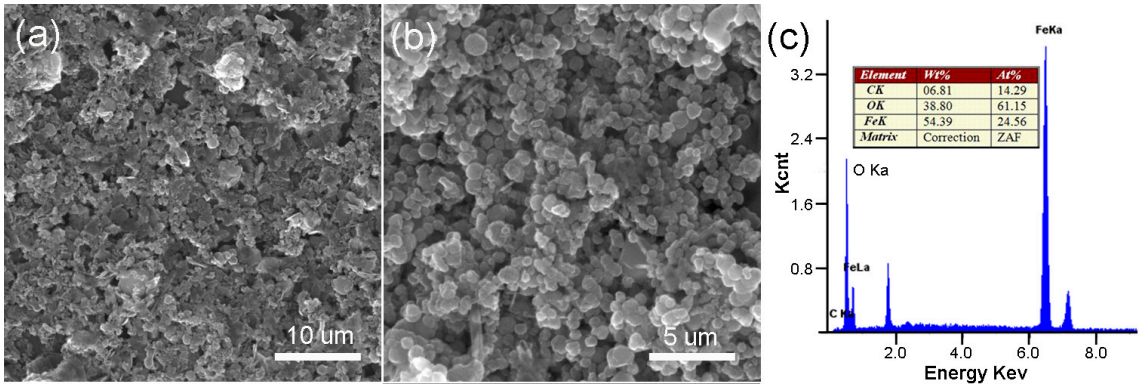

Figure 3. SEM (scanning electron microscopy) images of the r-GO/Fe_2O_3 NPs with different magnifications (**a**,**b**) and corresponding EDX (**c**).

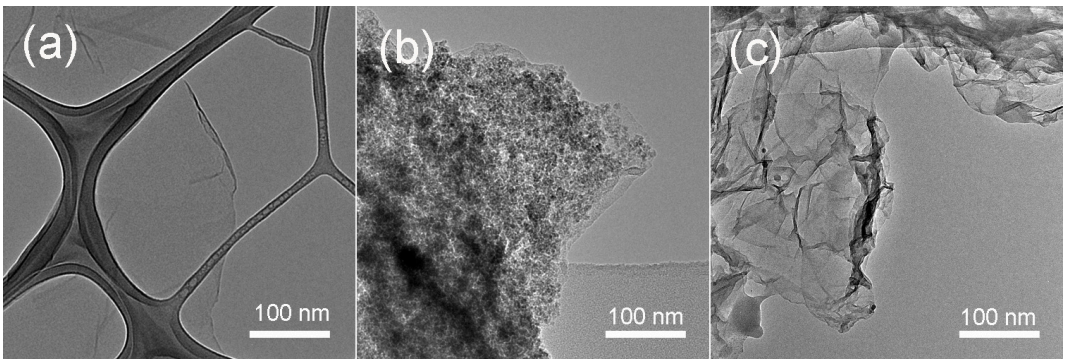

Figure 4. TEM (transmission electron microscopy) images of the (**a**) GO, (**b**) r-GO/Fe_2O_3, and (**c**) r-GO sheets.

Raman scattering is an important, non-destructive tool to characterize the change in the molecular structural of carbon based materials. The reducing process of GO was also investigated by Raman spectroscopy. The Raman spectrum (Figure 5) of GO showed two prominent peaks at 1355 and 1592 cm^{-1}, corresponding to the D band and G band, and the intensity ratio of D band to G band (I_D/I_G) which indicates the degree of the disorder such as defects, ripples, and edges [14] is approximately 0.64. The red curve is the Raman spectrum of r-GO/Fe_2O_3. Many peaks can be observed, which are located at 224, 242, 291, 406, 498, 609, and 1311 cm^{-1}, respectively [47]. All these peaks correspond to α-Fe_2O_3 phase. The Raman peaks appearing at 224 and 498 cm^{-1} are assigned to A_{1g} mode, and peaks at 291, 406, and 609 cm^{-1} are assigned to E_g modes. Meanwhile the peak observed at 1311 cm^{-1} is assigned to hematite two-magnon scattering. It is difficult to identify the carbon peak which should be located at ~1350 and ~1590 cm^{-1} because it has a strong fluorescent scattering of α-Fe_2O_3. After washed by HCl, other peaks between 200~1320 totally disappeared, showing that Fe_2O_3 NPs have been removed. On the contrary, the peaks of D and G band of carbon appeared and the I_D/I_G ratio of r-GO gradually increased to 1.19, which matches well with the results reported in the previous reports [12,14], indicating that GO has been reduced to r-GO completely.

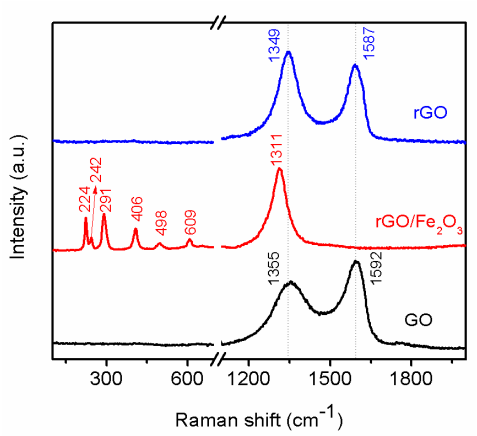

Figure 5. Raman spectra of GO, r-GO/Fe_2O_3, and r-GO.

The reduction process can also be detected by FTIR. The FTIR spectra (Figure 6) of GO showed peaks at 1072/1234 cm^{-1}, 1728 cm^{-1}, and 3449 cm^{-1} corresponding to the C–O, C=O, and –OH, which indicates there are lots of oxygenous groups on GO sheets. The FTIR spectra of r-GO showed the intensity of all peaks corresponding to the oxygenous groups decrease dramatically compared to that of primal GO, which further indicate GO nanosheets have been reduced to r-GO nanosheets [12].

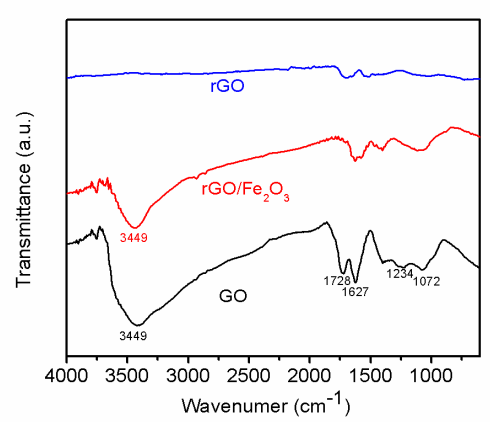

Figure 6. FTIR spectra of GO, r-GO/ Fe_2O_3, and r-GO.

3.3. Measure Nascent Hydrogen Reduction Efficiency

During the reduction process, many H atoms generated surrounding Fe_2O_3 NPs would quickly form H_2. By contrast, H_2 has no reducibility at room temperature [14]. Then a simple instrument was designed to collect H_2 produced and measure the content so as to quantify the reduction efficiency, as Figure 7 shows. The reduction ratios (H %) was calculated to be 43.6 % according to following formula:

$$H\ \% = 1 - \frac{V_{H_2-trapped}}{V_{H_2-theoretical}} \quad (3)$$

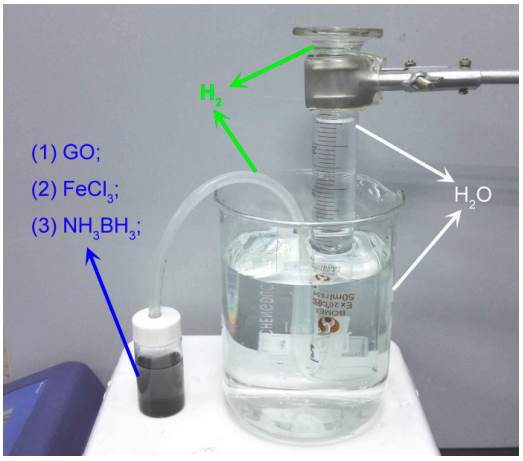

Figure 7. The instrument to measure the H_2 contends.

The reduction efficiency of different metal (Mg/Fe/Zn/Al) and acid reduction systems were also measured (Table 1). Compared to metal/acid reduction method, our method showed higher efficiency. It may be due to hydrophobic metal particles in the metal/acid system being unable to contact well with hydrophilic GO sheets. As a result, the nascent hydrogen which was formed around metal particles is tough to reduce GO sheets. In our method, much nascent hydrogen could be produced around the GO sheets surface as Fe_2O_3 NPs were in-site formed on the surface of GO sheets and could catalyze the hydrolysis of NH_3BH_3, thus GO was reduced more efficiently.

Table 1. Reduction efficiency of different metal/acid systems and our method.

Reduction Method	Raman (ID/IG)	H (%)	Reference
Mg/HCl	1.52	10.3	[38]
Fe/HCl	1.38	9.8	[35]
Zn/HCl	1.49	29.6	[36]
Al/HCl	1.32	7.2	[38]
NH_3BH_3/Fe_2O_3	1.19	43.6	this paper

3.4. Electrochemical Properties of r-GO

Due to the hydrophilic functional group is removed in the reduction process of GO, graphene nanosheets were easy to stack or aggregate so that the specific surface area was decreased. As a result, the capacitance of graphene nanosheets was reduced, which would limit its application in the fields of supercapacity. By our method, the gas generated in the reduction process could efficiently prevent nanosheets to aggregate and r-GO with porous structure was obtained (Figure 8).

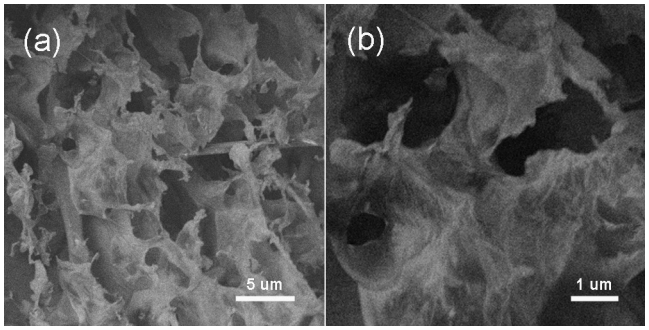

Figure 8. SEM images of the r-GO with different magnifications (**a**,**b**).

The electrochemical properties of r-GO were investigated by cyclic voltammetry (CV) test, in which 2 M KOH was worked as electrolyte. Figure 9 shows the CV curves of GO and r-GO at various scan rates of 5, 10, 20, 50, and 100 mV s^{-1}. The rectangular shape of the CV curves belong to r-GO can be attributed to good capacitive performance of the carbon based materials, and the current density of r-GO was 20 times as high as that of GO at the scan rate of 100 mV s^{-1}.

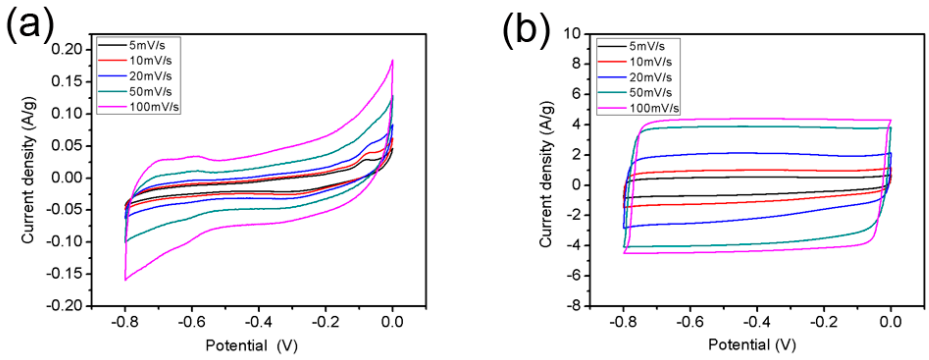

Figure 9. CV curves of GO (**a**) and r-GO (**b**) at various scan rates from 5 to 100 mV/s.

Rate capability test is important to evaluate the power performance of electrodes materials. Figure 10 shows the current galvanostatic discharge curves of r-GO electrode at different current densities. With the current density increase, shorter reaction time can be observed. Figure 11 shows the specific capacities of r-GO electrodes at current density of 1, 2, 5 and 10 A g^{-1}, respectively. It can be seen with the increase of current density, the capacity decrease from 113.8 F g^{-1} at 1 A g^{-1} to 96.25 F g^{-1} at 10 A g^{-1}. This can be attributed to the surface area of electrode contact with electrolyte reduced with the increase of current density.

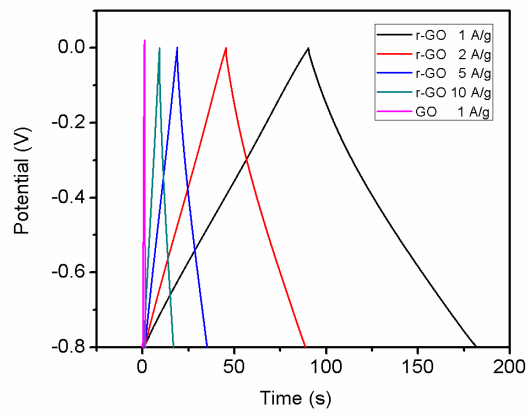

Figure 10. Galvanostatic charge–discharge curves of the symmetric supercapacitor at various current densities in 2 M KOH.

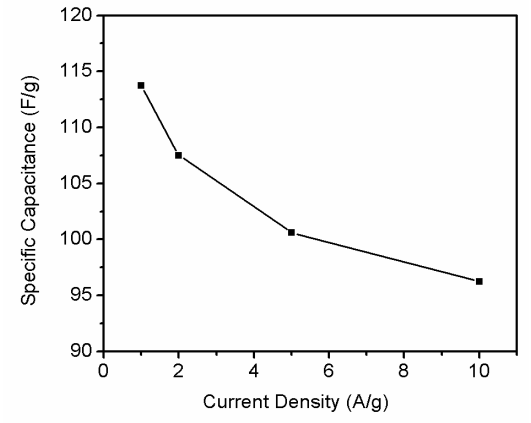

Figure 11. Specific capacitance of the symmetric supercapacitor at various current densities in 2 M KOH.

Cycling stability is another important supercapacitor parameter. Figure 12 shows the cyclic performances and specific retention of the r-GO electrodes at 1 A g^{-1}. After 200 cycles, the capacitance retention of the r-GO still remains at 90%, revealing that the electrodes exhibited good stability behaviors as supercapacitor electrode material.

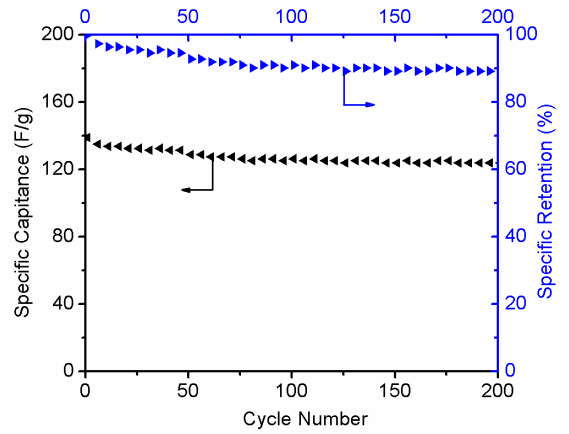

Figure 12. Cycling performance of r-GO electrodes at 1 A g^{-1} and specific retention.

4. Conclusions

Nascent hydrogen as an environmentally benign and strong reducing agent was used to efficiently reduction graphene oxide. In metal (Mg/Fe/Zn/Al) and acid reduction systems, hydrophobic metal powders and hydrophilic GO cannot contact well, which would result in low nascent hydrogen reduction ratio. In this article, a chemical method using Fe_2O_3 and NH_3BH_3 as catalyst and reductants was developed for high efficient reduction of GO. During the reduction process, Fe_2O_3 NPs were spontaneously formed on GO sheets surface due to the salting effect and catalyze the hydrolysis reaction of NH_3BH_3 to general nascent hydrogen at room temperature. The nascent hydrogen reduction ratio was up to 43.6%. Ultraviolet visible spectra, Fourier transform infrared spectrum, and Raman spectra demonstrated that almost all oxygenous groups on GO sheets were removed during the reduction process. As a supercapacitor electrode, the reversible capacity of reduced graphene oxide was 113.8 F g^{-1} at 1 A g^{-1} and the capacitance retention still remains at 90% after 200 cycles. Also the reaction was conducted at room temperature, which led to fewer defects during the reduction process. We expect that this method opens up a new way to reduce GO with high reduction efficiency and low defect under a mild condition.

Acknowledgments: This work was supported by general project of natural science foundation for high education insitutions in Jiangsu Province (15KJB430011) and policy guiding plan (university-industry cooperation)-prospective joint research project (BY2016073-02), six talent peaks project in Jiangsu Province (grant no. 2015-XCL-028). The authors also thank Yipeng Mao, Li Yu, Bolu Cui, Suwei Lu, and Hanzhao Wu collected the Raman, UV, and electrochemical data.

Author Contributions: Qiqi Zhuo conceived the study, designed the experiments, and wrote the paper; Jun Sun, Jijun Tang, and Chao Yan analyzed the data.

Conflicts of Interest: The authors declare no conflict of interest.

References

1. Wiederoder, M.S.; Nallon, E.C.; Weiss, M.; McGraw, S.K.; Schnee, V.P.; Bright, C.J.; Polcha, M.P.; Paffenroth, R.C.; Uzarski, J.R. Graphene Nanoplatelet-Polymer Chemiresistive Sensor Arrays for the Detection and Discrimination of Chemical Warfare Agent Simulants. *ACS Sens.* **2017**, *2*, 1669–1678. [CrossRef] [PubMed]
2. Ye, Z.B.; Tai, H.L.; Guo, R.; Yuan, Z.; Liu, C.H.; Su, Y.J.; Chen, Z.; Jiang, Y.D. Excellent ammonia sensing performance of gas sensor based on graphene/titanium dioxide hybrid with improved morphology. *Appl. Surf. Sci.* **2017**, *419*, 84–90. [CrossRef]
3. Choi, S.J.; Kim, S.J.; Jang, J.S.; Lee, J.H.; Kim, I.D. Silver Nanowire Embedded Colorless Polyimide Heater for Wearable Chemical Sensors: Improved Reversible Reaction Kinetics of Optically Reduced Graphene Oxide. *Small* **2016**, *12*, 5826–5835. [CrossRef] [PubMed]
4. Liu, C.H.; Chen, Q.; Zhong, Z.H. Graphene Ambipolar Nanoelectronics for High Noise Rejection Amplification. *Nano Lett.* **2016**, *16*, 1064–1068. [CrossRef] [PubMed]
5. Woo, J.; Yun, K.H.; Chung, Y.C. Graphene Monoxide Bilayer As a High-Performance on/off Switching Media for Nanoelectronics. *ACS Appl. Mater. Interfaces* **2016**, *8*, 10477–10482. [CrossRef] [PubMed]
6. Camilli, L.; Jorgensen, J.H.; Tersoff, J.; Stoot, A.C.; Balog, R.; Cassidy, A.; Sadowski, J.T.; Boggild, P.; Hornekaer, L. Self-assembly of ordered graphene nanodot arrays. *Nat. Commun.* **2017**, *8*, 47. [CrossRef] [PubMed]
7. Wei, L.; Karahan, H.E.; Zhai, S.L.; Liu, H.W.; Chen, X.C.; Zhou, Z.; Lei, Y.J.; Liu, Z.W.; Chen, Y. Amorphous Bimetallic Oxide-Graphene Hybrids as Bifunctional Oxygen Electrocatalysts for Rechargeable Zn-Air Batteries. *Adv. Mater.* **2017**, *29*, 1701410. [CrossRef] [PubMed]
8. Zhang, J.H.; Wan, S.; Yan, B.; Wang, L.B.; Qian, Y.T. Graphene Encapsulated Fe_3O_4 Nanospindles as a Superior Anode Material for Lithium-Ion Batteries. *J. Nanosci. Nanotechnol.* **2013**, *13*, 4364–4369. [CrossRef] [PubMed]
9. Liu, X.L.; Shou, D.; Chen, C.X.; Mao, H.H.; Kong, Y.; Tao, Y.X. Core-shell structured polypyrrole/mesoporous SiO_2 nanocomposite capped with graphene quantum dots as gatekeeper for irradiation-controlled release of methotrexate. *Mater. Sci. Eng. C Mater. Biol. Appl.* **2017**, *81*, 206–212. [CrossRef] [PubMed]
10. Jiang, W.L.; Zhou, W.; Ying, J.F.; Yang, T.Y.; Gao, Y.M. Thermal Stable Perovskite Solar Cells Improved by ZnO/Graphene Oxide as Electron Transfer Layers. *J. Inorg. Mater.* **2017**, *32*, 96–100. [CrossRef]
11. Xu, Y.H.; Li, J.; Huang, W.X. Porous Graphene Oxide Prepared on Nickel Foam by Electrophoretic Deposition and Thermal Reduction as High-Performance Supercapacitor Electrodes. *Materials* **2017**, *10*, 936. [CrossRef]
12. Zhuo, Q.Q.; Gao, J.; Peng, M.F.; Bai, L.L.; Deng, J.J.; Xia, Y.J.; Ma, Y.Y.; Zhong, J.; Sun, X.H. Large-scale synthesis of graphene by the reduction of graphene oxide at room temperature using metal nanoparticles as catalyst. *Carbon* **2013**, *52*, 559–564. [CrossRef]
13. Zhuo, Q.Q.; Ma, Y.Y.; Gao, J.; Zhang, P.P.; Xia, Y.J.; Tian, Y.M.; Sun, X.X.; Zhong, J.; Sun, X.H. Facile Synthesis of Graphene/Metal Nanoparticle Composites via Self-Catalysis Reduction at Room Temperature. *Inorg. Chem.* **2013**, *52*, 3141–3147. [CrossRef] [PubMed]
14. Zhuo, Q.Q.; Zhang, Y.P.; Du, Q.C.; Yan, C. Facile reduction of graphene oxide at room temperature by ammonia borane via salting out effect. *J. Colloid Interface Sci.* **2015**, *457*, 243–247. [CrossRef] [PubMed]
15. Strankowski, M.; Korzeniewski, P.; Strankowska, J.; A., S.A.; Thomas, S. Morphology, Mechanical and Thermal Properties of Thermoplastic Polyurethane Containing Reduced Graphene Oxide and Graphene Nanoplatelets. *Materials* **2018**, *11*, 82. [CrossRef] [PubMed]
16. Parviz, D.; Irin, F.; Shah, S.A.; Das, S.; Sweeney, C.B.; Green, M.J. Challenges in Liquid-Phase Exfoliation, Processing, and Assembly of Pristine Graphene. *Adv. Mater.* **2016**, *28*, 8796–8818. [CrossRef] [PubMed]

17. Arao, Y.; Mori, F.; Kubouchi, M. Efficient solvent systems for improving production of few-layer graphene in liquid phase exfoliation. *Carbon* **2017**, *118*, 18–24. [CrossRef]
18. Novoselov, K.S.; Geim, A.K.; Morozov, S.V.; Jiang, D.; Zhang, Y.; Dubonos, S.V.; Grigorieva, I.V.; Firsov, A.A. Electric field effect in atomically thin carbon films. *Science* **2004**, *306*, 666–669. [CrossRef] [PubMed]
19. Pang, J.B.; Mendes, R.G.; Wrobel, P.S.; Wlodarski, M.D.; Ta, H.Q.; Zhao, L.; Giebeler, L.; Trzebicka, B.; Gemming, T.; Fu, L.; et al. Self-Terminating Confinement Approach for Large-Area Uniform Monolayer Graphene Directly over Si/SiO_X by Chemical Vapor Deposition. *ACS Nano* **2017**, *11*, 1946–1956. [CrossRef] [PubMed]
20. Chen, Z.P.; Wang, H.I.; Teyssandier, J.; Mali, K.S.; Dumslaff, T.; Ivanov, I.; Zhang, W.; Ruffieux, P.; Fasel, R.; Rader, H.J.; et al. Chemical Vapor Deposition Synthesis and Terahertz Photoconductivity of Low-Band-Gap N=9 Armchair Graphene Nanoribbons. *J. Am. Chem. Soc.* **2017**, *139*, 3635–3638. [CrossRef] [PubMed]
21. Tripathi, K.; Gyawali, G.; Lee, S.W. Graphene Coating via Chemical Vapor Deposition for Improving Friction and Wear of Gray Cast Iron at Interfaces. *ACS Appl. Mater. Interfaces* **2017**, *9*, 32336–32351. [CrossRef] [PubMed]
22. Hummers, W.S.; Offeman, R.E. Preparation of graphitic oxide. *J. Am. Chem. Soc.* **1958**, *80*, 1339. [CrossRef]
23. Ramabadran, U.; Ryan, G.; Zhou, X.; Farhat, S.; Manciu, F.; Tong, Y.G.; Ayler, R.; Garner, G. Reduced Graphene Oxide on Nickel Foam for Supercapacitor Electrodes. *Materials* **2017**, *10*, 1295. [CrossRef] [PubMed]
24. Stankovich, S.; Dikin, D.A.; Piner, R.D.; Kohlhaas, K.A.; Kleinhammes, A.; Jia, Y.; Wu, Y.; Nguyen, S.T.; Ruoff, R.S. Synthesis of graphene-based nanosheets via chemical reduction of exfoliated graphite oxide. *Carbon* **2007**, *45*, 1558–1565. [CrossRef]
25. Singh, R.K.; Kumar, R.; Singh, D.P. Graphene oxide: strategies for synthesis, reduction and frontier applications. *RSC Adv.* **2016**, *6*, 64993–65011. [CrossRef]
26. Zhao, X.; Xu, Z.; Xie, Y.; Zheng, B.; Kou, L.; Gao, C. Polyelectrolyte-Stabilized Graphene Oxide Liquid Crystals against Salt, pH, and Serum. *Langmuir* **2014**, *30*, 3715–3722. [CrossRef] [PubMed]
27. Kim, J.E.; Han, T.H.; Lee, S.H.; Kim, J.Y.; Ahn, C.W.; Yun, J.M.; Kim, S.O. Graphene Oxide Liquid Crystals. *Angew. Chem. Int. Ed.* **2011**, *50*, 3043–3047. [CrossRef] [PubMed]
28. De Silva, K.K.H.; Huang, H.H.; Joshi, R.K.; Yoshimura, M. Chemical reduction of graphene oxide using green reductants. *Carbon* **2017**, *119*, 190–199. [CrossRef]
29. Zhou, X.J.; Zhang, J.L.; Wu, H.X.; Yang, H.J.; Zhang, J.Y.; Guo, S.W. Reducing Graphene Oxide via Hydroxylamine: A Simple and Efficient Route to Graphene. *J. Phys. Chem. C* **2011**, *115*, 11957–11961. [CrossRef]
30. Shin, H.-J.; Kim, K.K.; Benayad, A.; Yoon, S.-M.; Park, H.K.; Jung, I.-S.; Jin, M.H.; Jeong, H.-K.; Kim, J.M.; Choi, J.-Y.; et al. Efficient Reduction of Graphite Oxide by Sodium Borohydride and Its Effect on Electrical Conductance. *Adv. Funct. Mater.* **2009**, *19*, 1987–1992. [CrossRef]
31. Lei, Z.B.; Lu, L.; Zhao, X.S. The electrocapacitive properties of graphene oxide reduced by urea. *Energy Environ. Sci.* **2012**, *5*, 6391–6399. [CrossRef]
32. Zhu, C.; Guo, S.; Fang, Y.; Dong, S. Reducing sugar: new functional molecules for the green synthesis of graphene nanosheets. *ACS Nano* **2010**, *4*, 2429–2437. [CrossRef] [PubMed]
33. Zhang, J.; Yang, H.; Shen, G.; Cheng, P.; Zhang, J.; Guo, S. Reduction of graphene oxide vial-ascorbic acid. *Chem. Commun.* **2010**, *46*, 1112. [CrossRef] [PubMed]
34. Zhang, Z.; Chen, H.H.; Xing, C.Y.; Guo, M.Y.; Xu, F.G.; Wang, X.D.; Gruber, H.; Zhang, B.L.; Tang, J.L. Sodium Citrate: A Universal Reducing Agent for Reduction/Decoration of Graphene Oxide with Au Nanoparticles. *Nano Res.* **2011**, *4*, 599–611. [CrossRef]
35. Fan, Z.J.; Kai, W.; Yan, J.; Wei, T.; Zhi, L.J.; Feng, J.; Ren, Y.M.; Song, L.P.; Wei, F. Facile Synthesis of Graphene Nanosheets via Fe Reduction of Exfoliated Graphite Oxide. *ACS Nano* **2011**, *5*, 191–198. [CrossRef] [PubMed]
36. Liu, P.; Huang, Y.; Wang, L. A facile synthesis of reduced graphene oxide with Zn powder under acidic condition. *Mater. Lett.* **2013**, *91*, 125–128. [CrossRef]
37. Fan, Z.J.; Wang, K.; Wei, T.; Yan, J.; Song, L.P.; Shao, B. An environmentally friendly and efficient route for the reduction of graphene oxide by aluminum powder. *Carbon* **2010**, *48*, 1686–1689. [CrossRef]
38. Sofer, Z.; Jankovsky, O.; Simek, P.; Soferova, L.; Sedmidubsky, D.; Pumera, M. Highly hydrogenated graphene via active hydrogen reduction of graphene oxide in the aqueous phase at room temperature. *Nanoscale* **2014**, *6*, 2153–2160. [CrossRef] [PubMed]
39. Ramachandran, P.V.; Gagare, P.D. Preparation of ammonia borane in high yield and purity, methanolysis, and regeneration. *Inorg. Chem.* **2007**, *46*, 7810–7817. [CrossRef] [PubMed]

40. Sun, D.; Mazumder, V.; Metin, O.; Sun, S. Methanolysis of Ammonia Borane by CoPd Nanoparticles. *ACS Catal.* **2012**, *2*, 1290–1295. [CrossRef]
41. Hamilton, C.W.; Baker, R.T.; Staubitz, A.; Manners, I. B-N compounds for chemical hydrogen storage. *Chem. Soc. Rev.* **2009**, *38*, 279–293. [CrossRef] [PubMed]
42. Yao, Q.; Shi, W.; Feng, G.; Lu, Z.-H.; Zhang, X.; Tao, D.; Kong, D.; Chen, X. Ultrafine Ru nanoparticles embedded in SiO2 nanospheres: Highly efficient catalysts for hydrolytic dehydrogenation of ammonia borane. *J. Power Sources* **2014**, *257*, 293–299. [CrossRef]
43. Kalidindi, S.B.; Indirani, M.; Jagirdar, B.R. First row transition metal ion-assisted ammonia-borane hydrolysis for hydrogen generation. *Inorg. Chem.* **2008**, *47*, 7424–7429. [CrossRef] [PubMed]
44. Akbayrak, S.; Ozkar, S. Ruthenium(0) Nanoparticles Supported on Multiwalled Carbon Nanotube As Highly Active Catalyst for Hydrogen Generation from Ammonia-Borane. *ACS Appl. Mater. Inter.* **2012**, *4*, 6302–6310. [CrossRef] [PubMed]
45. Xi, P.; Chen, F.; Xie, G.; Ma, C.; Liu, H.; Shao, C.; Wang, J.; Xu, Z.; Xu, X.; Zeng, Z. Surfactant free RGO/Pd nanocomposites as highly active heterogeneous catalysts for the hydrolytic dehydrogenation of ammonia borane for chemical hydrogen storage. *Nanoscale* **2012**, *4*, 5597–5601. [CrossRef] [PubMed]
46. Lapin, N.V.; D'Yankova, N.Y. Hydrogen evolution kinetics during transition metal oxide-catalyzed ammonia borane hydrolysis. *Inorg. Mater.* **2013**, *49*, 975–979. [CrossRef]
47. Hassan, M.F.; Rahman, M.M.; Guo, Z.P.; Chen, Z.X.; Liu, H.K. Solvent-assisted molten salt process: A new route to synthesise alpha-Fe_2O_3/C nanocomposite and its electrochemical performance in lithium-ion batteries. *Electrochim. Acta* **2010**, *55*, 5006–5013. [CrossRef]